Journal of Physics: Conference Series **154** (2009) 012038 doi:10.1088/1742-6596/154/1/012038

Gravitational disturbances in drag-free spacecraft

Antonio Pulido Patón[1*], Clive C Speake[2], Christian Trenkel[3], Sachie Shiomi[4] and Wei-Tou Ni[1]

[1]Center for Gravitation and Cosmology, Purple Mountain Observatory, Chinese Academy of Sciences, Beijing West Road 2, Nanjing 210008, P. R. China.
[2]School of Physics and Astronomy, University of Birmingham, Edgbaston, Birmingham B15 2TT, United Kingdom.
[3]Astrium UK, Gunnels Wood Road, Stevenage, Hertfordshire, SG1 2AS, United Kingdom.
[4]Space Geodesy Laboratory, Department of Civil Engineering, National Chiao Tung University, Hsinchu, Taiwan, 300, ROC.

E-mail: *antonio@pmo.ac.cn

Abstract. The performance of drag-free spacecraft will be ultimately limited by the uncompensated gravitational field and gravity field gradient of the spacecraft structure and payload. We identify sources of disturbance of gravitational origin and we explore a new concept for determining gravitational fields in the vicinity of the proof mass. The benefits of these diagnostic tools for future missions, like ASTROD, are discussed.

1. Introduction

Geodesic motion is at the core of numerous space-borne experimental tests of Gravity and Fundamental Physics. Tests of the Equivalence Principle and the Gravitational Inverse Square Law, the identification of the nature of the Pioneer Anomaly, measurements of the Gravitational Constant and its spatial-temporal variations, tests of relativistic gravity, i.e., light deflection and light retardation, geodesic deviation and Lense-Thirring effect, and the detection and measurement of gravitational waves, are within the most fundamental experimental searches in Gravitation theory. To perform such tests, proof masses in free fall are generally required. The technique to place a proof mass in geodesic/free-fall motion is known as drag-free technology.

Currently the state-of-the-art technology in drag-free performance presumes that we can achieve an acceleration noise in free-fall motion with an accuracy of about 3×10^{-14} m s^{-2} Hz$^{-1/2}$, in the measurement bandwidth between 1 mHz and 30 mHz. This is the acceleration noise performance expected for the LTP (LISA Technology Package) in the mission LISA Pathfinder [1]. LISA Pathfinder is the technology precursor of the LISA (Laser Interferometer Space Antenna) mission [2]. On the other hand, other mission concepts like ASTROD (Astrodynamical Space Tests of Relativity using Optical Devices) [3] aims at improving drag-free performance compared to LISA at frequencies below the LISA MBW, i.e., up to micro-hertz frequencies, while the Japanese gravitational wave antenna DECIGO (DECi-hertz Interferometer Gravitational wave Observer) [4] requires drag-free performance at deci-hertz frequencies.

It is worth noticing that the verification of an anomalous acceleration towards the Sun, the Pioneer Anomaly, requires DC drag-free performance. Also in the case of the ASTROD mission concept, the measurement of the relativistic parameter β, and the determination of

the asteroids masses require long integration times and therefore DC or quasi-DC drag-free performance is beneficial. The idea of designing a space capsule with a near zero gravitational force acting on the test bodies had previously been considered within the project SEE (Satellite Energy Exchange). The SEE project [5] aims to measure the gravitational constant and its time variation by measuring the gravitational energy exchange between two bodies.

In this paper, we consider the self-gravity effects in inertial sensors. The presence of residual local gravitational fields is an obstacle for further improvement of drag-free performance. Local gravity gradients couple the proof mass to the spacecraft contributing to the acceleration noise because of spacecraft jittering and structural distortion. Local gravity fields are also a key requirement in order to achieve high drag-free performance at DC. In what follows we discuss new ideas about plausible gravitational diagnostic tools to actively tune drag-free performance in orbit.

2. Gravitational disturbances

In the current state-of-the-art drag-free technology, the coupling of the proof mass and the spacecraft is mainly due to residual electrostatic and local gravitational gradients. Electrostatic couplings are caused by proximity of metallic surfaces to the proof mass. Nevertheless electrostatic sensors, commonly used in drag-free satellites, require close gaps to achieve high sensitivity. Electrostatic sensing is also intrinsically unstable, and, therefore, we face the problems related to the need for low-frequency force feedback for ultra low-frequency drag-free operation. To solve these problems, optical sensors have been considered for implementation in the next-generation drag-free spacecraft [6, 7]. Given that scenario, drag-free performance will then be limited by the spacecraft self-gravitational field. To suppress gravitational noise we must identify its origin and, if possible, we have to introduce gravitational diagnostic tools and compensation techniques. Here is a list of possible sources of gravitational noise:

- Thermal and other distortions of the spacecraft and payload. Thermal-gravitational effects contribute as a fluctuating force noise [8] and they are likely to shift the local gravitational field value. There could also be some distortions due to, for example, tidal effects [9].
- Gravitational force and gradients due to micrometeorites passing nearby the spacecraft [10].
- Changes of the local gravitational field due to asymmetrical thruster propellant consumption.
- Changes of the local gravitational field due to active thermal control techniques (i.e. movable radiation panels, changing phase materials for absorption and rejection of heat, etc).
- Changes of the local gravitational field due to the need to move payload constituents (i.e. communicating antennae, moving telescopes for laser beam pointing, etc).
- Gravitational noise due to density inhomogeneities of the proof mass and defects in the constructing materials. Density inhomogeneities in the proof mass induce, to first order, residual proof mass dipole and quadrupole moments. These moments are coupled to the spacecraft gravitational gradients. In drag-free spacecraft, the proof mass is fixed in position and orientation, and ideally located in a minimum of the local gravitational potential. In that case, noise caused by density inhomogeneities is minimized.

In the case of ASTROD, some of the spacecraft will be exposed to a significant change of solar irradiance flux due to variations of spacecraft-Sun relative distance. Given that scenario, the spacecraft are likely to require active thermal control techniques. In the ASTROD constellation, the line of sight between one of the spacecraft and the distant spacecraft varies along the orbit. That will affect the spacecraft self-gravity due to the need to move the telescopes for laser beam pointing. In a preliminary design, dummy telescopes are considered to compensate this change of gravitational field at the proof mass location. The fact that spacecraft self-gravity could change

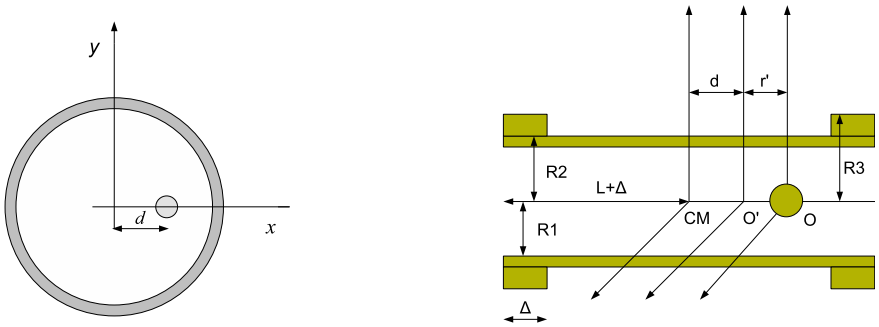

Figure 1. Gravity gradiometer concept for gravitational diagnostic in drag-free spacecraft. The inner proof mass of the gradiometer is in free fall motion and it is inserted inside an outer mass shell. The gravitational field inside the spherical outer mass shell vanishes whatever the position the proof mass inside the shell (left). Alternative gravity gradiometer configuration with a cylindrical-type outer mass shell geometry (right).

along the orbit is an important motivation to explore gravitational diagnostic techniques. In what follows, we describe a gravity gradiometer to measure "in situ" the local gravitational field at the free-falling proof mass location.

3. Gravity diagnostic tools

A standard drag-free spacecraft, which employs only one proof mass, can not monitor the spacecraft self-gravitational field gradients. The idea of a gravity gradiometer for an inertial sensor is shown in figure 1. The proof mass in drag-free motion lies inside an outer mass shell. The outer mass shell must fulfill two requirements: (a) it should provide a second reference mass to measure gravitational gradients; and (b) the outer mass shell should not contribute to the local gravitational field acting on the proof mass. To achieve the former, the center of mass of the inner and outer masses have to be shifted with respect to each other. By suppressing the acceleration experienced by the inner mass due to "internal" gravity in the gradiometer, the spacecraft gravitational gradients are monitored by measuring the differential acceleration (or displacement) of the inner mass relative to the outer shell. With (b) we ensure that the gravitational gradient measured is due to the surrounding spacecraft. We also need to eliminate coupling to gradients and higher orders of the outer shell gravitational potential below the gravity gradient noise requirement. Gravitational gradiometers with outer spherical and cylindrical shells are depicted in figure 1. An obvious appealing property of the spherical geometry (figure 1 (left)) is that the local gravitational field is zero whatever the proof mass position inside the shell.

3.1. A gravity gradiometer for self-gravity diagnostic

Due to manufacturing and engineering difficulties in constructing a spherical shell, we explore other non-spherical geometries with similar properties. We consider the cylindrical-type outer shell geometry shown in figure 1 (right). To start the discussion it is useful to think of the proof mass acceleration as due to a multipole expansion around the origin. The proof mass acceleration along an axis, in terms of multipole moments, is given by [11],

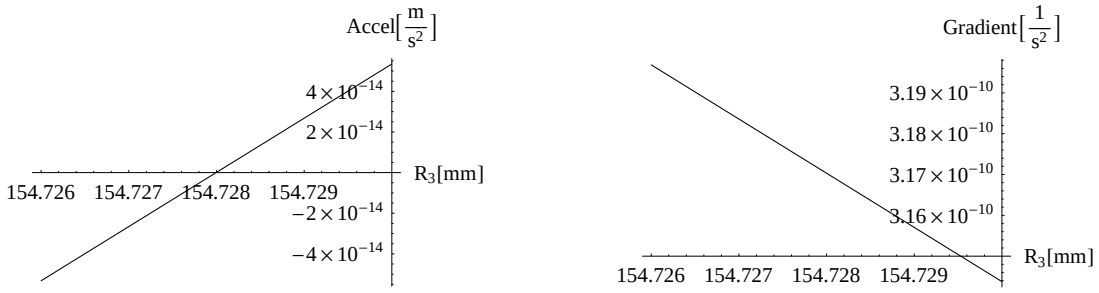

Figure 2. The inner mass acceleration due to the outer shell is zero for a value of $R_3 \simeq 154.728$ mm (left). The residual gravity gradient is of the order of 3×10^{-10} s^{-2} (right). The geometry parameters are chosen to be L=200, R_1=100, R_2=120, Δ=80 and d=20 milimeters.

$$a_z = \frac{4\pi G}{M_{tm}} \sum_{l=1}^{\infty} \sum_{m=-l}^{+l} \sqrt{\frac{(l-m)(l+m)}{(2l-1)(2l+1)}} q_{l-1,m} Q_{lm} \tag{1}$$

where M_{tm} is the mass of the inner test body, q_{lm} are the inner multipole moments of the test mass and Q_{lm} are the outer multipole moments of the outer shell. By inspection of equation (1), we conclude that the axial field, a_z, can be made small by eliminating as many multipole terms in the expansion as possible. For the purposes of this work, it is more convenient to use the following expansion of the gravitational potential for a cylindrically symmetric outer mass shell. If we restrict ourselves to displacements of a point test mass along the axis of symmetry we find that (see Appendix A)

$$V(z) = -G(4\pi)^{1/2} q_{00} \sum_{L=0}^{\infty} \sqrt{\frac{4\pi}{2L+1}} Q_{L0} z^L \tag{2}$$

where z defines the displacement of the proof mass with respect to the operating position. It should be noticed (see figure 1) that the operating position of the free-falling proof mass is shifted by a distance d with respect to the center of mass of the outer shell. In equation (2) the outer multipoles, Q_{LM}, are calculated with respect to the reference frame with origin at O' (see figure 1 (right) and appendix A for explanation). It is also interesting to note that in general the outer multipoles of a body can be calculated about an arbitrary origin following [12]. Equation (2) shows that the gravitational gradient is proportional to outer shell multipole Q_{20}. As mentioned above, the gravitational field inside the outer spherical shell geometry vanishes whatever the position of the inner proof mass inside the shell. If we consider an infinitely long hollow cylinder the gravitational field is also zero whatever the proof mass position inside the shell. This is not the case when we consider a hollow cylinder of finite length. However we can design a "stepped" cylindrical geometry (see figure 1 (right)) for which the local acceleration, proportional to Q_{10}, can be made zero given the right parameter values. A drawback of that geometry is that the inner mass will be in unstable equilibrium on the cylinder axis. Stabilizing forces should then be applied passively or actively. As a comment, here we are trying to design a hollow cylinder which behaves gravitationally like a spherical shell in the inside region by eliminating its outer multipoles, Q_{LM}. That can be compared with, for example, the test masses design strategy for the STEP (Satellite Test of the Equivalence Principle) mission [13]. The geometry of the STEP test masses is chosen to eliminate the inner multipoles, q_{lm}, in order to construct monopole test masses.

For a "sufficiently" far away spacecraft structure and payload, the masses configuring the gravity gradiometer can be considered as point masses. In that approximation, we can estimate

the sensitivity to spacecraft gravity gradients, K_{gg}, by the ratio of the residual differential acceleration between the inner and outer mass, due to their internal gravitational interaction, and the center of mass separation, d, i.e. $\Delta a_{res} \simeq K_{gg} d$. Figure 2 (left) shows a particular set of geometrical parameters for which we have a zero local acceleration. However because of machining inaccuracies and inaccuracy in center of mass knowledge and positioning, the acceleration has an uncertainty of the order of 10^{-13} m s^{-2}. We have considered those inaccuracies to be at the micrometer level. With this particular choice of parameters the expected sensitivity to "external" gravity gradients is about 5×10^{-12} s^{-2}. The residual gravitational gradient due to the outer shell is about 3×10^{-10} s^{-2} (see figure 2 (right)). These numbers are sufficiently below the allocated magnitude of the uncertainty in $K_{gg} \sim 3 \times 10^{-8}$ s^{-2} for ASTROD I [14].

In a practical scheme we envisage being able to modulate the spacecraft gravity field acting on the gradiometer by periodically changing the position of the spacecraft using the thrusters. Active correction and nulling of the asymmetry in the mass distribution could be accomplished using trim masses.

4. Conclusions

In the next generation of drag-free spacecraft the ultimate obstacle to improve the quality of geodesic motion will be the residual self-gravity field at the location of the free-falling proof mass. Gravitational diagnostic tools on ground and/or in orbit will be of demand for future drag-free spacecraft. We have emphasized that a standard drag-free spacecraft with one proof mass only, is unable to measure the spacecraft self-gravitational field gradient. Measurement of the gravity gradient may serve to help distinguish between gravitational and non-gravitational interactions between the drag free sensor and the spacecraft. We have proposed a gravity gradiometer with two masses, one of which is the free-falling proof mass, to measure "in situ" the self-gravitational field at the proof mass location. The relative motion of the inner and outer masses will be most likely measured interferometrically.

Acknowledgments

One of the authors (APP) has been supported by CAS Research Fellowship for International Young Researchers, grant no. 20070309. We (APP and WTN) would like to thank the National Natural Science Foundation of China (grant nos. 10705051, 10778710) for supporting this work.

Appendix A. Multipole expansion of the gravitational potential

We describe the gravitational interaction between an inner test mass and an outer mass shell (see figure 1) by means of a spherical harmonic expansion. In the general case, the gravitational potential energy between two rigid bodies in terms of multipole moments can be written as

$$V = -4\pi G \sum_{L=0}^{\infty} \sum_{M=-L}^{+L} \frac{1}{2L+1} \tilde{q}_{LM} Q_{LM} \tag{A.1}$$

where $\tilde{q}_{LM}(Q_{LM})$ are the inner(outer) multipoles defined by

$$\tilde{q}_{LM} = \int_{v_t} \rho_t r'^L Y^*_{LM}(\Theta', \Phi') d^3x' \quad \text{and} \quad Q_{LM} = \int_{v_s} \rho_s r^{-(L+1)} Y_{LM}(\Theta, \Phi) d^3x \tag{A.2}$$

and (r', Θ', Φ'), (r, Θ, Φ) refer to spherical coordinates of the inner and outer test masses. The density distributions, ρ_t and ρ_s, are assumed to be uniform. The multipoles are calculated in the same reference frame, in our case with origin at O' according to figures 1 (right) and A1.

By performing a translation of the inner multipole in equation (A.1), we can infer how the gravitational potential energy varies around O'. Following [15] we express the inner multipoles

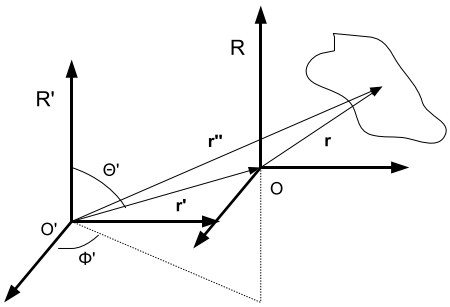

Figure A1. Reference frames to calculate the gravitational potential multipole expansion.

$\tilde{q}_{LM}$, calculated with respect to reference frame R' with origin at O', in terms of the inner multipoles q_{lm}, calculated with respect to the reference frame R with origin at O (see figure A1) as

$$\tilde{q}_{LM} = \sum_{l,l'=0}^{L} \sum_{m,m'} \sqrt{\frac{4\pi(2L+1)!}{(2l+1)!(2l'+1)!}} r'^{l'} \delta_{L,l+l'} C(l',m',l,m,L,M) Y^*_{l'm'}(\hat{r}') q_{lm} \tag{A.3}$$

By substituting (A.3) into (A.1), the potential energy can be written in terms of the translation parameter, r', and the direction (Θ', Φ') of the translation giving

$$V(r',\Theta',\Phi') = -4\pi G \sum_{L=0}^{\infty} \sum_{M=-L}^{+L} \frac{1}{2L+1} Q_{LM}$$
$$\sum_{l,l'=0}^{L} \sum_{m,m'} \sqrt{\frac{4\pi(2L+1)!}{(2l'+1)!(2l+1)!}} C(l',m',l,m,L,M) \delta_{L,l+l'} r'^{l'} Y^*_{l',m'}(\Theta',\Phi') q_{lm} \tag{A.4}$$

For the case of an inner monopole mass performing a displacement along the symmetry axis of a cylindrical shell, the equation (A.4) transforms into equation (2).

References

[1] McNamara P *et al* 2008 *Class. Quantum Grav.* **25** 114034
[2] Bell T E 2008 *Nature* **452** 7183 18
[3] Ni W T 2008 *Int. J. Mod. Phys.* D **17**(7) 921
[4] Kawamura S *et al* 2006 *Class. Quantum Grav.* **23** S125
[5] Sanders A J *et al* 1999 Meas. Sci. Technol. **10** 514
[6] Xu X and Ni W T 2003 *Adv. Space Res.* **32**(7) 1443
[7] Speake C C and Aston S M 2005 *Class. Quantum Grav.* **22** S269
[8] Stebbins R T *et al* 2004 *Class. Quantum Grav.* **21** S653
[9] Scheithauer S *et al* 2006 *Class. Quantum Grav.* **23** 7273
[10] Purdue P and Larson S L 2007 *Class. Quantum Grav.* **24** 5869
[11] Shiomi S *et al* 2001 *Class. Quantum Grav.* **18** 2533
[12] Trenkel C and Speake C C 1999 *Phys. Rev.* D **60** 107501-2
[13] Mester J 2001 *Class. Quantum Grav.* **18** 2475
[14] Shiomi S and Ni W T 2006 *Class. Quantum Grav.* **23** 4415
[15] D'Urso C and Adelberger E G 1997 *Phys. Rev.* D **55** 7970